Extensional rheology of shear-thickening nanoparticle suspensions

Manojkumar Chellamuthu, Eric M. Arndt and Jonathan P. Rothstein*

Received 19th November 2008, Accepted 27th February 2009
First published as an Advance Article on the web 20th April 2009
DOI: 10.1039/b820684h

A filament-stretching rheometer is used to measure the extensional properties of shear-thickening nanoparticle suspensions as a function of concentration and extension rate. The experiments are performed using a series of colloidal suspensions consisting of concentrations of 17.5 wt%, 25 wt% and 30 wt% of fumed silica nanoparticles in polypropylene glycol. The shear rheology of these suspensions was found to demonstrate dynamic shear-thickening behavior owing to the formation of large hydrodynamic clusters. The critical value of angular frequency for the onset of shear-thickening was found to increase monotonically with decreased strain amplitude. The extensional rheology of all the tested suspensions demonstrated modest strain-hardening at low strain rates. At a critical extension rate, a dramatic increase in both the speed and magnitude of the strain-hardening is observed for both the 25 wt% and 30 wt% suspensions with increasing extensional rate. The steady state extensional viscosity as a function of extension rate shows sharp extensional thickening transition very similar to shear flows. The increase in strain-hardening is likely due to the formation of strings and clusters ordered in the flow direction. This hypothesis is confirmed by small-angle light scattering measurements of the flow of the nanoparticle suspension through a microfluidic hyperbolic contraction. The degree of alignment of nanoparticles is quantified from the analysis of the scattering patterns and found to increase significantly with increasing extension rate.

I. Introduction

The early investigations of shear-thickening systems were inspired by the damage often caused to the processing equipment and the dramatic changes in suspension microstructure which were found to often result in poor fluid and coating qualities.[1] A great deal of research has been dedicated to understanding and predicting the dynamics of shear-thickening colloidal suspensions.[1–11] The use of shear-thickening fluids has resulted in a tremendous amount of industrial and commercial innovations. As an example, the highly nonlinear behavior of shear-thickening fluids has been exploited in the design of machine mounts and damping devices.[12,13] Additionally, it has recently been demonstrated that shear-thickening fluids, when incorporated into bullet-proof vests and subjected to high velocity projectiles, can dramatically improve both the performance and flexibility of body armor.[10]

The origins of shear-thickening in colloidal suspensions have been debated in the recent literature. In his pioneering work,[2] Hoffman used light diffraction combined with shear rheology to investigate micro-structural details during the onset of shear-thickening. He proposed that the onset of shear-thickening at the critical shear rate corresponds to an order-to-disorder transition of particles. In subsequent years, researchers have simulated and experimentally studied different types of colloidal dispersions to investigate the validity of the proposed order to disorder transition. Boersma *et al.*[8] proposed a new model for the onset of shear-thickening on the basis of balance between hydrodynamic shear forces and stabilizing electrostatic force which agreed with the dynamic simulation proposed by Bossis *et al.*[14] for the hydrodynamic clustering of particles. Their experimental investigations agreed well with their proposed critical shear rate dependence on medium viscosity, particle radius and the volume fraction. Bossis and Brady[15] determined the viscosity of a suspension of spherical Brownian particles by Stokesian dynamics as a function of the Peclet number. According to their simulation results, the suspensions shear-thicken at high Peclet numbers due to the formation of large clusters. Other experimental studies[1,16–19] have also confirmed that shear-thickening can occur without shear-induced order to disorder transition. Through measurements of rheology, turbidity, flow small-angle neutron scattering and stress–optical relationship, Bender *et al.*[1] showed that hydrodynamic lubrication forces dominates all the other colloidal forces in the shear-thickened suspension and concluded that shear-thickening results from a transition from a shear-induced ordered structure to the state of hydrodynamic clustering. The important parameters that controls the shear-thickening are particle size distribution, particle shape, particle–particle interactions and viscosity of suspended phase.[3] The cumulative effects of these parameters controls the pre- and post-transition response of the shear-thickening phenomenon.[11]

A number of researchers have investigated the dynamic properties of shear-thickening fluids.[6,11,13,20–22] Laun *et al.*[13] investigated the flow properties of a strongly shear-thickening polymer dispersion in steady, transient and oscillatory shear flows. Their oscillatory measurements demonstrated that the transition to shear-thickening occurred at a critical strain amplitude, γ_c, which decreased with increasing angular frequency, ω. More recently, Boersma *et al.*[20] studied the viscoelastic behavior of concentrated dispersions of silica particles suspended in a mixture of glycerol and water. From

Department of Mechanical and Industrial Engineering, University of Massachusetts, Amherst, MA, 01003, USA

the oscillatory shear measurements, they interpreted the low frequency behavior in terms of a steady shear response, where the critical shear rate ($\dot{\gamma}_c^{dynamic} = \gamma_c^{\omega} = \dot{\gamma}_c^{steady}$) must be attained in order for the suspension to shear-thicken. Using this modified Cox-Merz rule, also known as the Delaware-Rutgers rule, the data for both oscillatory and steady shear flows can be collapsed on to a single master curve. The agreement between steady shear and low frequency dynamic oscillatory response was supported by Bender and Wagner[23] through optical measurements on hard-sphere dispersions. Raghavan and Khan[6] also confirmed the agreement for systems very similar to those used in this study. According to their results, fumed silica suspensions in low molecular weight polypropylene glycol (PPG) exhibit shear-thickening at high critical strains and low frequencies. The hydrodynamic interactions between two nanoparticles are proportional to the dynamic shear rate. At moderate frequencies, the hydrodynamic forces overcome the repulsive interactions between particles resulting in the connection of aggregates at the critical dynamic shear rate to form clusters. At high frequencies, the hydrodynamic forces get large enough to break down clusters and the fluids begin to shear-thin again.

Although shear rheology of thickening suspensions are well understood, the extensional rheology of these suspensions remains mostly unexplored. Only a very limited number of studies have investigated the response of suspensions to extensional flows. Xu *et al.*[24] investigated the morphology and rheology of an entangled nanofiber/glycerol-water suspensions containing millimeter- and centimeter-size agglomerates. They used an opposed jet device to investigate a 1 wt% nanofiber suspensions under extensional flow. The suspensions exhibit extensional thinning behavior which is likely a result of breakdown of entangled nanofiber network structure under extensional stress. Ma *et al.*[25] used capillary breakup extensional rheometry to investigate the difference in extensional rheology of a Newtonian epoxy, and a series of suspensions of carbon nanotubes in the epoxy. The extensional viscosity measurements were in good agreement with theoretical predictions of Batchelor[26] and Shaqfeh *et al.*[27] who studied rigid rod particles in extensional flows. The extensional viscosity enhancement observed for carbon nanotube suspensions is the result of orientation of carbon nanotube in the flow direction during the stretch. In this work, we compare the shear and extensional rheology of suspensions of fumed silica particles suspended in low molecular weight polypropylene glycol. To understand the extensional properties of these suspensions, we systematically investigated the effect of concentration of the colloidal suspensions and extension rate using a filament-stretching rheometer and correlate the results to light scattering measurements made using a microfluidic hyperbolic contraction.

The outline of the paper is as follows. In Section II, we briefly describe the implementation of the filament-stretching extensional rheometer, flow cell design for the light scattering experiments and test fluids used. In Section IIIA, we compare and discuss the extensional rheology of the test fluids measured using filament-stretching rheometer with shear rheology measurements. In Section IIIB, we discuss the light scattering measurements obtained from flow cell to help interpret the extensional rheology of test fluids. Finally, in Section IV we conclude.

II. Experimental setup

A. Test fluids

A series of suspensions of concentrations 17.5 wt%, 25 wt% and 30 wt% were prepared by mixing hydrophilic fumed silica (Aerosil® 200, Evonik Degussa) in polypropylene glycol with M_n = 1000 g/mol (Aldrich) in a blender. The hydrophilic fumed silica has a primary particle size of 12 nm and has a specific surface area of approximately 200 m^2/g. These primary particles are irreversibly fused to form large aggregates, typically about 100 nm in size. These aggregates are branched chain-like structure with an aspect ratio that appears to be on average about 5:1 and characteristic fractal dimension, d_f equal to 1.7 in three-dimensional space.[6] Images of these particles can be found in Raghavan *et al.*[6] After one hour of mixing, the suspension, a transparent and colorless liquid, was obtained. The resulting suspensions were kept in the vacuum chamber for several hours to remove the air bubbles before use.

B. Filament-stretching rheometry

A filament-stretching extensional rheometer (FiSER) capable of imposing a homogeneous uniaxial extension on a fluid filament placed between its two endplates, was used to make measurements of the evolution in the force and the midpoint radius simultaneously. A complete description of the design and operating space of the filament-stretching rheometer used in these experiments can be found in refs. 28 and 29, and a more detailed history of the technique can be found in papers by the McKinley and Sridhar groups.[30–32] The goal of extensional rheometry is to produce a motion such that the resulting extension rate imposed on the fluid filament, $\dot{\varepsilon}$, is constant. The deformation imposed upon the fluid filament can be described in terms of a Hencky strain, $\varepsilon = -2\ln(R_{mid}/R_0)$,where R_0 is the initial midpoint radius of the fluid filament. The strength of the extensional flow is characterized by the Weissenberg number, $Wi = \lambda\dot{\varepsilon}$, which is the ratio of the characteristic relaxation time of the fluid, λ to the characteristic timescale of the flow, $1/\dot{\varepsilon}_0$. The elastic tensile stress difference generated within the filament, $\langle \upsilon_{zz} - \upsilon_{rr} \rangle$ can be calculated from the force measured by the load cell, if the weight of the fluid and the surface tension are taken into account while ignoring inertial effects:[33]

$$\langle \tau_{zz} - \tau_{rr} \rangle = \frac{F_z}{\pi R_{mid}^2} + \frac{1}{2}\frac{\rho(\pi L_0 R_0^2)}{\pi R_{mid}^2} - \frac{\sigma}{R_{mid}} \quad (1)$$

The extensional viscosity may be extracted from the principle elastic tensile stress, $\eta_E = \langle \upsilon_{zz} - \upsilon_{rr} \rangle/\dot{\varepsilon}$, and is often non-dimensionalized as a Trouton ratio, $Tr = \eta_E/\eta_0$.

C. Hyperbolic contraction flow cell design

In order to investigate the structure formation and alignment of the nanoparticle suspension in extensional flows, small-angle light scattering (SALS) experiments were performed. Unfortunately, the curvature of a stretching fluid filament and the resulting lensing of an incident laser beam made it impossible to perform light scattering during a filament-stretching experiment. In order to produce a nearly uniform extensional flow of the

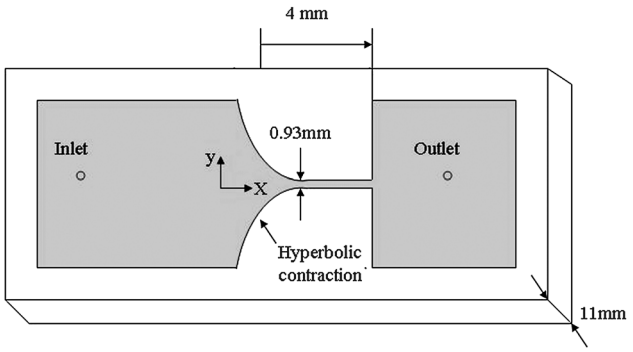

Fig. 1 Schematic diagram of the hyperbolic contraction used to perform light scattering measurements.

silica suspension in a manner that affords analysis by small-angle light scattering, an acrylic flow cell containing a hyperbolic contraction was constructed and is shown in Fig. 1. A long length of the channel before the hyperbolic contraction was fabricated to guarantee a fully developed flow. The contraction was constructed as a set of precision-machined acrylic inserts. The hyperbolic profile is governed by

$$y = \frac{c_1}{x + c_2}, \tag{2}$$

where y is the half-width of the channel measured from the channel midpoint, x is the position measured from the beginning of the hyperbolic contraction, and c_1 and c_2 are constants which can be set to change the strength of the extensional flow produced.

In an ideal case, where the flow slips along the walls of the flow cell and plug flow is achieved, a constant extension rate is achieved everywhere in the channel. This can be seen by a simple analysis of the flow. The velocity at any point in the channel is $u = u_0 y_0 / y$, where u_0 and y_0 are the velocity and channel width at the entrance to the contraction. The extension rate then becomes

$$\dot{\varepsilon} = \frac{\partial u}{\partial x} = u_0 y_0 c_1.$$

Of course, such an idealized flow does not occur and a constant rate in the absence of shear cannot be achieved; however, a nearly constant extension rate can still be achieved along the centerline of the hyperbolic contraction.[34] To ensure that our light-scattering measurements were measuring changes resulting from extensional and not shear-thickening, a value of $c_1 = 1.86$ mm^2 and $c_2 = 0.075$ mm was chosen such that the shear rate everywhere in the hyperbolic contraction was smaller than the critical shear rate for the onset of shear-thickening. This limited the flow rates and extension rates that could be used, but was sufficient to fully probe extension rates up to the extensional thickening dynamics for the 25 wt% case. Overall, the hyperbolic contraction allowed us to probe extension rates up to $\dot{\varepsilon} = 10$ s^{-1}and an accumulated strains of $\varepsilon = 4.0$.

A 250 mA diode laser (red, 600–700 nm) was used for the small-angle light scattering setup. This laser was positioned above the hyperbolic contraction at a number of positions along the centerline of the channel corresponding to different accumulated strains. A 400 μm pinhole was used to reduce the beam size and allow for precise measurement. The scattering pattern was projected onto a piece of white paper located 46 cm below the flow cell. A Nikon D70 camera was mounted on a tripod and used to capture images of the scattering patterns.

III. Results and discussions

A. Shear rheometry

The steady and dynamic shear rheology of the test fluids were characterized using a stress-controlled rheometer (TA instruments, AR2000) with 40 mm parallel plate geometry. The suspensions were loaded and allowed to equilibrate for several minutes. In Fig. 2, the Delaware-Rutgers rule, $\eta^*(\gamma_0\omega) = \eta(\dot{\gamma})$, is applied to collapse the data from dynamic frequency sweeps at different set strains ranging from 50% to 1000%. The steady-shear viscosity data is superimposed over the dynamic data. All the tested nanoparticle suspensions were observed to initially shear-thin at lower strain and strain rates and shear-thicken at higher strain and strain rates, presumably owing to the formation of large hydrodynamic clusters.[6] These hydrodynamic clusters are composed of groups of particles formed as shear forces drive them to contact, and short-range lubrication forces dominate the flow resulting in a viscosity increase.[1] The shear-thickening transition is initiated at lower frequencies when the strain amplitude is high. The critical value of angular frequency for the onset of shear-thickening was found to increase monotonically with decreased strain amplitude. These observations are consistent with previous work involving similar colloidal systems,[6,11] although the concentrations tested here are in some cases larger than those reported in the literature.

B. Filament-stretching rheometry

A series of transient extensional rheology measurements were performed on the silica particle suspensions with concentrations of 17.5 wt%, 25 wt% and 30 wt%. In Fig. 3, a series of representative plots of extensional viscosity as a function of accumulated Hencky strain is presented for a series of extension rates, varying from $\dot{\varepsilon} = 1$ s^{-1} to $\dot{\varepsilon} = 7$ s^{-1}. As seen in Fig. 3, only a modest strain-hardening is observed at low strain rates. In this regime, the extensional rheology is essentially insensitive to changes in extension rate and is similar to the response of nanofiber suspensions made in the past where enhancement of the extensional viscosity was due to alignment of the high aspect ratio fibers in the flow direction.[25] The nanoparticles used in this study are not spherical, but are fractal, with a chain-like structure resulting from fusion of many spherical primary particles into a single aggregate particle. As a result they have a modest aspect ratio which can appear to be as much as 10:1 from the SEM images presented in Raghavan *et al.*[6] One would therefore expect some extensional thickening resulting from alignment of individual nanoparticles in the flow direction, as has been observed in experiments and predicted for suspensions of rigid rods. For the 17.5 wt% concentration shown in Fig. 3a, a similar response was observed at all the extension rates tested. However, at critical extension rate of $\dot{\varepsilon} = 5.5$ s^{-1}and $\dot{\varepsilon} = 2.0$ s^{-1}, a dramatic increase in both the speed and magnitude of the strain-hardening is observed for the 25 wt% and 30 wt% solutions (Fig. 3b and 3c, respectively) with increasing extensional rate.

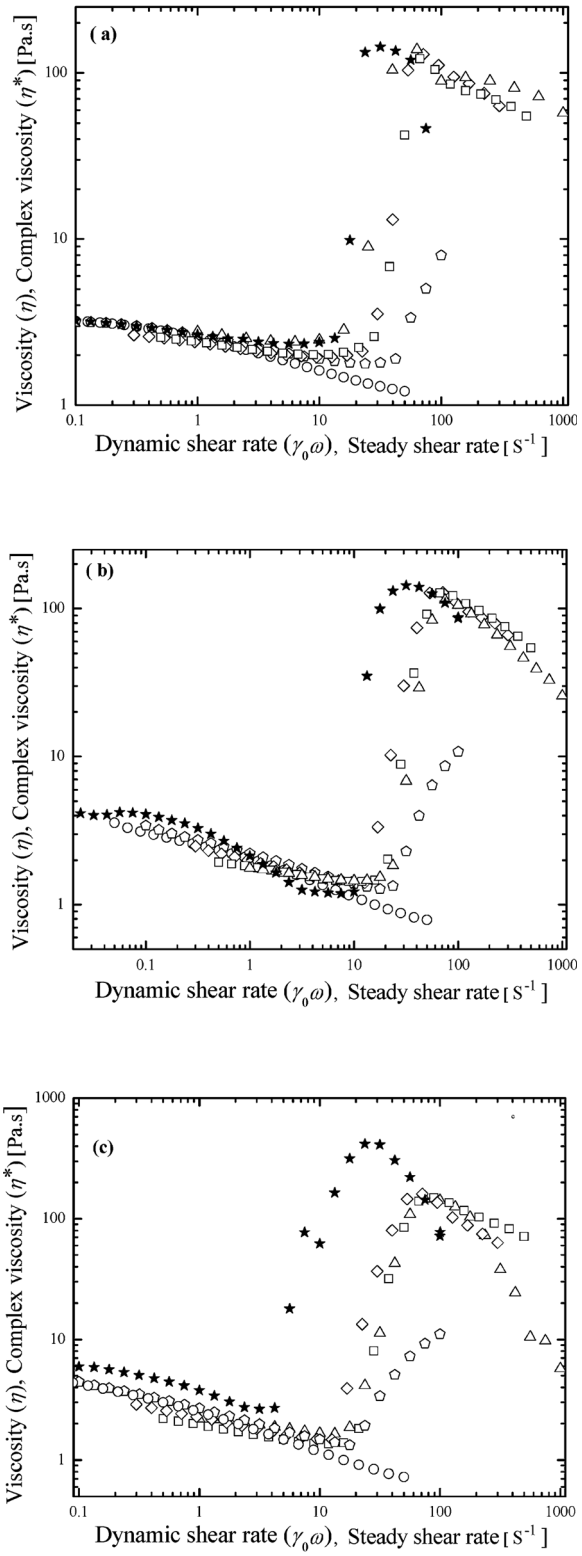

Fig. 2 Delaware-Rutgers rule [$\eta^*(\gamma_0\omega) = \eta(\dot{\gamma})$] applied to the data from dynamic frequency sweeps at different set strains (γ_0) 50% (○) 100% (⬠), 300% (◇), 500% (□), 1000% (△) and steady strain-rate sweeps (★). The data included in are (a) 17.5 wt%, (b) 25 wt% and (c) 30 wt% colloidal suspensions of silica in polypropylene glycol.

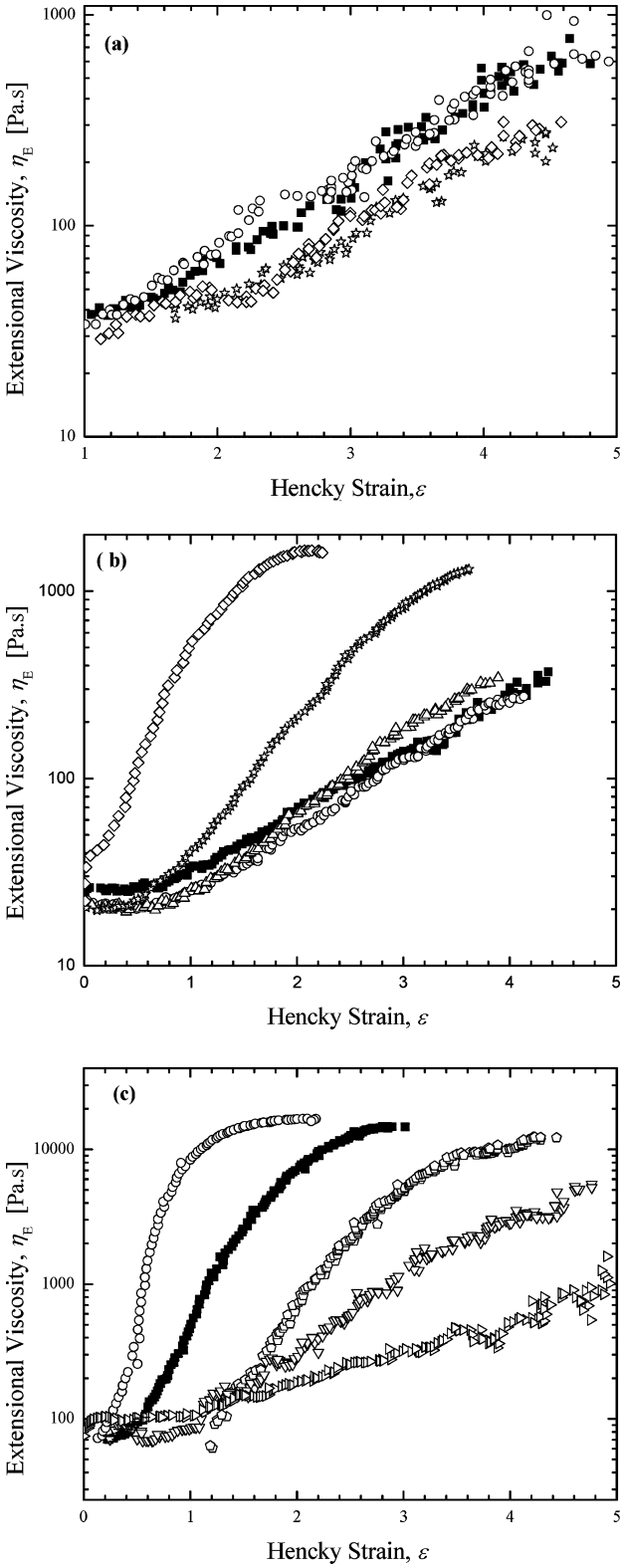

Fig. 3 FiSER measurements of the transient extensional viscosity as a function of accumulated Hencky strain for different concentrations of silica suspensions in polypropylene glycol at $T = 23$ °C. Included in (a) are solutions of 17.5 wt% with extension rates $\dot{\varepsilon} = 4\ s^{-1}$ (■), $5\ s^{-1}$ (○), $6\ s^{-1}$ (☆), $7\ s^{-1}$ (◇) while in (b) are solutions of 25 wt% with extension rates $\dot{\varepsilon} = 4\ s^{-1}$ (■), $5\ s^{-1}$ (○), $5.5\ s^{-1}$ (△), $6\ s^{-1}$ (☆), $7\ s^{-1}$ (◇) and in (c) are solutions of 30 wt% with extension rates $\dot{\varepsilon} = 1\ s^{-1}$ (▷), $2\ s^{-1}$ (▽), $3\ s^{-1}$ (⬠), $4\ s^{-1}$ (■), $5\ s^{-1}$ (○).

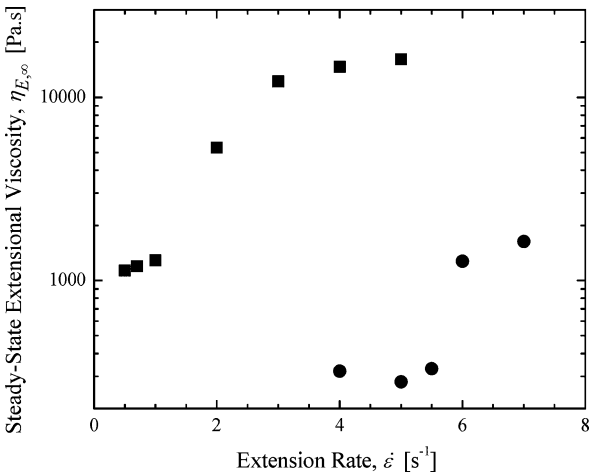

Fig. 4 Steady-state extensional viscosity as a function of extension rate for 30 wt% (■) and 25 wt% (●) silica suspensions in polypropylene glycol at $T = 23$ °C.

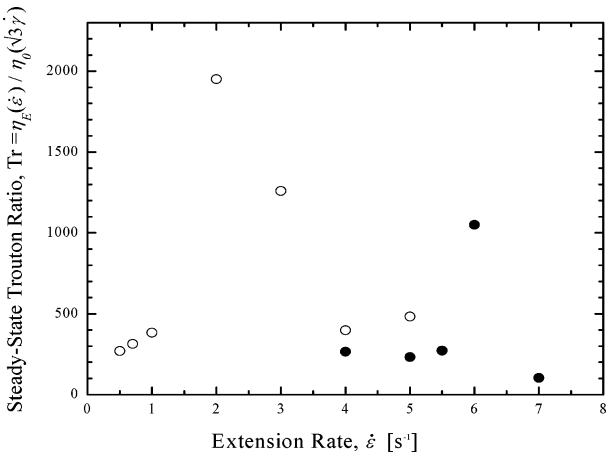

Fig. 5 Steady-state Trouton ratio as a function of extension rate for 30 wt% (○) and 25 wt% (●) colloidal suspensions of silica in polypropylene glycol.

The sharpness of the extensional rheology transition observed in Fig. 3 is extraordinary. In both polymeric and wormlike micelle solutions, the steady-state extensional viscosity is observed to increase and the onset of strain-hardening has been observed to move towards smaller strains with increasing extension rate.[31,35] However, in neither of those cases is such a dramatic or quick transition in extensional viscosity is observed. Take for example, the 30 wt% solution in Fig. 3c. At a Hencky strain at $\varepsilon = 1$, the extensional viscosity is found to increase from approximately $\eta_E = 100$ Pa s to $\eta_E = 1000$ Pa s to $\eta_E = 9000$ Pa s as the extension rate is increased from $\dot{\varepsilon} = 3\ s^{-1}$ to $\dot{\varepsilon} = 4\ s^{-1}$ to $\dot{\varepsilon} = 5\ s^{-1}$. With less than a 70% increase in extension rate an increase in the extensional viscosity of two orders of magnitude was observed. We believe that this dramatic increase in strain-hardening is likely due to the same mechanism responsible for shear-thickening in shear flows; the formation of long nanoparticle strings ordered and aligned in the flow direction, where interparticle interactions dominate the flow leading to an increased viscosity. To emphasize the similarity between the shear and extensional measurements, the steady-state extensional viscosity is plotted in Fig. 4 as a function of extension rate for both the 25 wt% and 30 wt% nanoparticle suspensions. The steady state extensional viscosity in Fig. 4 shows a sharp extensional thickening transition which is very similar in magnitude to the shear-thickening transition observed in steady shear flows. In all likelihood, if we could have stretched the filament faster, a similar transition might have been observed for the 17.5 wt% suspension.

A natural question that arises is whether the observed extensional thickening is a new phenomena or simply a manifestation of the same physical mechanism that resulted in the thickening observed in shear. In order to compare the relative magnitude of extensional to shear-thickening, the Trouton ratio is shown as a function of extension rate in Fig. 5. The Trouton ratio is defined using the convention proposed by Jones *et al.*,[36] $Tr = \eta_E(\dot{\varepsilon})/\eta(\dot{\gamma} = \sqrt{3}\dot{\varepsilon})$, where the shear viscosity used to normalize the steady-state extensional viscosity is evaluated at a shear rate of $\dot{\gamma} = \sqrt{3}\dot{\varepsilon}$. This definition will always give a conservative estimate of the Trouton ratio. Even after taking shear-thickening effects into consideration, a steep rise in steady-state Trouton ratio is observed for both 25 wt% and 30 wt% colloidal suspensions. Extensional hardening is thus observed to occur at deformation rates smaller than those found to result in shear-thickening. For example, in the 30 wt% case, the value of the steady-state Trouton ratio is observed to increase an order of magnitude as the extension rate is increased from $\dot{\varepsilon} = 0.5\ s^{-1}$ to $\dot{\varepsilon} = 2\ s^{-1}$ before returning to more modest values at higher extension rates.

These observations clearly demonstrate that based on the critical deformation rate for the onset of thickening, extensional flows are more effective than shear flows at forming and aligning strings of nanoparticles. This observation may be surprising at first because a strong extensional flow might be expected to break down weakly aggregated structures. However, the relative rheological enhancement in extensional flows as compared to shear flows might be attributable to the lack of rotation in extensional flow which could be responsible for slowing the formation or even breaking down long string-like nanoparticle aggregates in shear flows. Although the thickening occurs at lower deformation rates in extensional flows, the thickening transition occurs at a significantly higher stress in extensional flows. This is quantified in Table 1 through a comparison of the critical shear stress, $\upsilon_{yx,c}$, and extensional stress, $(\upsilon_{zz} - \upsilon_{rr})_c$, for the onset of shear and extensional thickening of colloidal suspensions as a function of particle concentration. An important observation from Table 1 is that both the critical shear and extensional stresses are found to decay approximately linearly with increasing concentration. This suggests that the physical mechanism for shear and extensional thickening is the same.

To explore the sensitivity of formation of strings of particles in extensional flows, we used a pre-shear device attached to the

Table 1 Critical shear strees, $\upsilon_{yx,c}$, and extensional stress, $(\upsilon_{zz} - \upsilon_{rr})_c$, for the onset of shear and extensional thickening of colloidal suspensions of fumed silica in polypropylene glycol

Particle concentration/wt%	$\upsilon_{yx,c}$/Pa	$\dot{\gamma}_c/s^{-1}$	$(\upsilon_{zz} - \upsilon_{rr})_c$/Pa	$\dot{\varepsilon}_c/s^{-1}$
17.5	24	13	>2400	>7
25	13	10	1800	5.5
30	11	5	1300	2

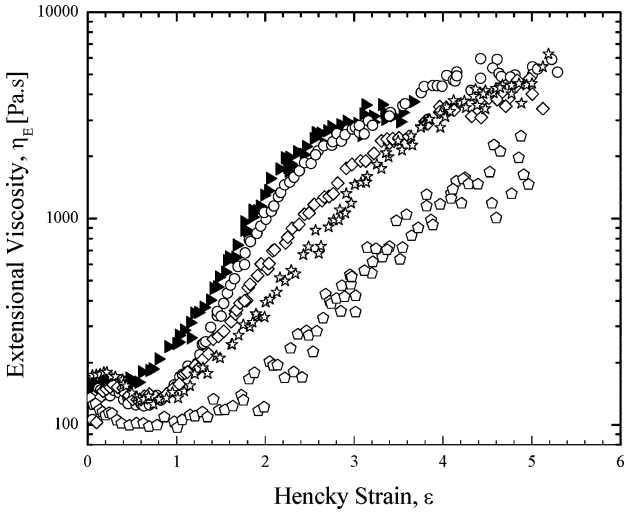

Fig. 6 Extensional viscosity with varying pre-shear rates $\dot{\gamma} = 0.3\ s^{-1}$ (○), $0.6\ s^{-1}$ (◇), $1\ s^{-1}$ (☆), $3\ s^{-1}$ (⬠) as a function of accumulated Hencky strain for 30 wt% colloidal suspensions of silica in polypropylene glycol with fixed extension rate of $\dot{\varepsilon} = 1s^{-1}$. The filled (►) corresponds to case without pre-shear.

upper endplate of our filament-stretching rheometer as described in Bhardwaj *et al.*[37] Using this device, the test fluids were subjected to shear rates varying in strength from $\dot{\gamma} = 0.3$ to $3s^{-1}$ for a fixed duration of ten seconds just prior to the onset of stretch. In Fig. 6, the extensional viscosity with different pre-shear strengths and fixed extension rates of $\dot{\varepsilon} = 1\ s^{-1}$ and $4\ s^{-1}$ is plotted as a function of accumulated Hencky strain for the 30 wt% colloidal suspensions. In Fig. 6, we can see that the extensional viscosities with low pre-shear strength more or less behave like a pure extensional flow. However, with increasing pre-shear strength there is a delay in the onset of extensional thickening transition. We believe that the formation of strings of particles at higher pre-shear strengths tend to delay the onset of extensional thickening, because the aligned strings must be rotated from the shear direction into the extensional direction before strain-hardening can begin. Similar observations have been made for the extensional viscosities of polymer solutions[38,39] and wormlike micelle solutions in extensional flows following pre-shear.[37]

B. Small-angle light scattering

As described in Section IIC, a hyperbolic contraction was used to investigate the alignment and ordering of nano-particle suspensions in extensional flows through small-angle light scattering measurements. In Fig. 7, the SALS patterns are shown for extension rates of $\dot{\varepsilon} = 0$, 5 and $8\ s^{-1}$ for the 25 wt% colloidal suspensions. All images in Fig. 7 are taken at a position in the hyperbolic contraction where the suspensions have accumulated a total strain of $\varepsilon = 2$. Below an extension rate of $\dot{\varepsilon} = 5\ s^{-1}$, the scattering pattern is indistinguishable from the no-flow case. For $\dot{\varepsilon} \geq 5\ s^{-1}$, a bright streak appears in the scattering pattern normal to the flow direction. It is important to note that the range of scattering vectors that we could interrogate with our SALS setup was between $0.5 < q < 3.8\ \mu m^{-1}$. Within this range, information about the alignment of the individual chainlike nanoparticles could not be obtained because they are too small. Thus only

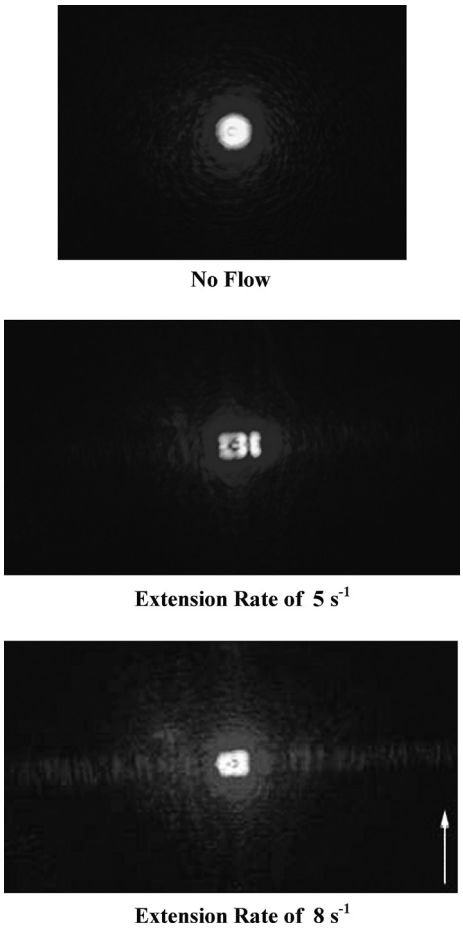

Fig. 7 Small-angle light scattering patterns for 25 wt% colloidal suspensions of silica in polypropylene glycol flowing through a micro-fluidic hyperbolic contraction designed to produce a nearly constant extension rate flow. Scattering for three different extension rates all at a location in the hyperbolic contraction corresponding to an accumulated strain of $\varepsilon = 2$. The arrow indicates the flow direction.

scattering from aggregates of particles could be observed. The scattering patterns observed in Fig. 7 are indicative of the formation of long strings of particles aligned in the flow direction.[40] As seen in Fig. 7, the intensity and length of this streak in the scattering pattern increases with increasing extension rate. The onset of alignment of strings or aggregated strings is observed to begin at extension rate of $\dot{\varepsilon} = 5\ s^{-1}$, which corresponds to the onset of the dramatic extensional hardening in Fig. 3.

In Fig. 8, the normalized pixel intensity is shown as a function of azimuthal angle, ϕ, for SALS patterns shown in Fig. 7. It is clear from Fig. 8, the alignment of clusters in the flow direction is demonstrated by the peak in the pixel intensity at $-90°$ and $90°$. Here the flow is aligned with $0°$. The strength of the peak and therefore the degree of string alignment is observed to increase with extension rate. In Fig. 9, the scattering intensity, I, is plotted as a function of the scattering vector, q, for the three extension rates presented in Fig. 7. The variation of scattering intensity with scattering vector for all the extension rates tested were found to be indistinguishable from the no-flow case. Fits to the decay in scattering intensity using a hard-sphere structure model

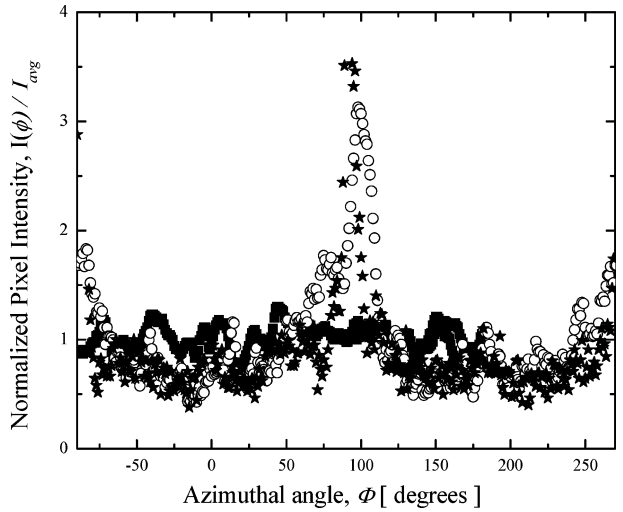

Fig. 8 Normalized pixel intensity of the scattering images presented in Fig. 7 as a function of azimuthal angle for 25 wt% colloidal suspensions of silica in polypropylene glycol. Included are solutions for no flow (■), and extension rates of 5 s^{-1} (○) and 8 s^{-1} (★).

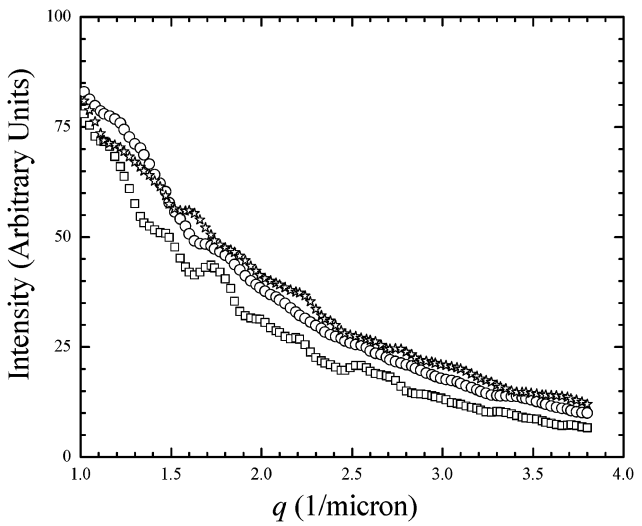

Fig. 9 Intensity of the scattering images presented in Fig. 7 as a function of scattering vector, q for 25 wt% colloidal suspensions of silica in polypropylene glycol. Included are solutions for no flow (□), and extension rates of 5s^{-1} (○) and 8s^{-1} (☆).

produced comparable interparticle spacings. We did not observe any correlation peaks that could further our understanding of the early onset of cluster and string formation. However, this was not completely unexpected given the large concentration of particles in our solutions and the relatively large length-scales that can be probed by our small-angle light scattering apparatus. The interaction of individual particles to produce clusters is a small length-scale phenomena that would require much higher wave vectors to be probed.[41] In our future studies, we hope to use neutron scattering or ultra-small-angle light scattering to gain more insight into the onset of hydrodynamic clustering in extensional flows.

In order to quantify the alignment of the strings of nanoparticles, the scattering intensity, $I(q,\phi)$, is weighted by

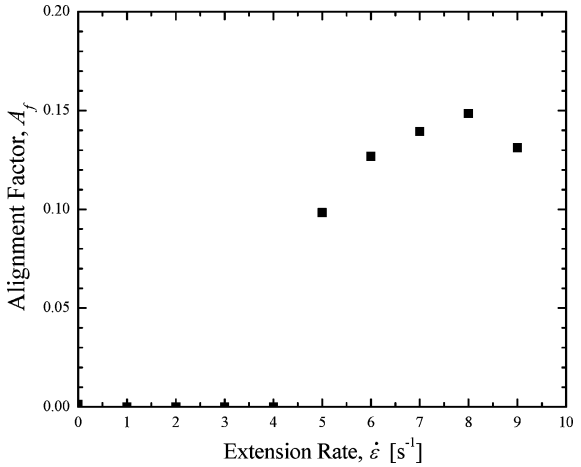

Fig. 10 Alignment factor as a function of extension rate for 25 wt% colloidal suspensions of silica in polypropylene glycol. All measurements are taken at a location in the hyperbolic contraction corresponding to an accumulated strain of $\varepsilon = 2$.

a spherical harmonic to capture the degree of asymmetry in the scattering. The result is an alignment factor defined as[40,42]

$$A_f(q) = \frac{\int_0^{2\pi} I(q,\phi)\cos(2\phi)\,\mathrm{d}\phi}{\int_0^{2\pi} I(q,\phi)\,\mathrm{d}\phi} \qquad (2)$$

In Fig. 10, we present a value of the alignment factor averaged over a finite range of the scattering vector between $0.5 \leq q \leq 3.8\ \mu m^{-1}$. In our experiments, $\phi = 0°$ is the flow direction. The alignment factor ranges from $A_f = 0$ for an unaligned sample to $A_f = 1$ for a perfectly aligned sample. For uniaxially aligned rigid rods, the alignment factor has been shown to be equivalent to the macroscopic order parameter.[42] The alignment factor is calculated as a function of extension rate for 25 wt% colloidal suspensions and plotted in Fig. 9. The magnitude of alignment is observed to increase from 0 to 0.14 as the extension rate is increased to 9 s^{-1}. The alignment factor appears to plateau or perhaps even decrease a little for extension rates above $\dot{\varepsilon} = 8\ s^{-1}$. These results are very much in agreement with Fig. 2b, where we can observe dramatic increase in strain-hardening for these extension rates. The scattering clearly demonstrates that the extensional thickening is due to the rapid alignment of strings of particles in flow direction as the extension rate increases beyond $\dot{\varepsilon} = 5\ s^{-1}$. Unlike the scattering of Scirocco *et al.*,[40] who observed Bragg scattering patterns corresponding to a dilute suspension of polystyrene particles nicely aligned with uniformly spaced strings of particles in shear flow, we saw no such patterns. However, the alignment factors measured in our experiments are quite similar to those reported by Scirocco *et al.*[40]

Conclusions

The extensional properties of shear-thickening colloidal suspensions of silica in polypropylene glycol were studied using a filament-stretching rheometer as a function of concentration and extension rate. The shear rheology of a series of suspensions of concentrations 17.5 wt%, 25 wt% and 30 wt% demonstrated

a shear-thinning behavior at low strain and strain rates and shear-thicken at high strain and strain rates owing to the formation of large hydrodynamic clusters. The shear-thickening transition was observed to be initiated at lower frequencies when the strain amplitude was high. The critical value of angular frequency for the onset of shear-thickening was found to increase monotonically with decreased strain amplitude. These observations are consistent with previous work involving similar colloidal systems.

A series of extensional rheology measurements were performed on suspensions of concentrations 17.5 wt%, 25 wt% and 30 wt% using filament-stretching rheometry. The extensional rheology of all the tested suspensions demonstrated modest strain-hardening at low strain rates. For both the 30 wt% and the 25 wt% nanoparticle suspensions, the extensional rheology was found to be insensitive changes in extension rate in the low strain rate regime. However, at a critical extension rate, a dramatic increase in both the rate and magnitude of the strain-hardening was observed for the 25 wt% and 30 wt% suspensions with increasing extensional rate. This observed strain-hardening is similar in form to the shear rheology. The steady-state extensional viscosity showed a sharp extensional thickening transition with increasing extension rate very similar to that observed in shear flows. This dramatic increase in strain-hardening is most likely due to the formation of strings aligned in the flow direction, similar to the mechanism postulated to explain the shear-thickening of these fluids.

The formation of strings and alignment of clusters are quite sensitive to pre-shear strengths prior to extension. The extensional viscosities with low pre-shear strength more or less behave like pure extension flow. However, with increase in pre-shear strength after critical pre-shear strength, there is a sharp delay in the onset of extensional thickening transition. The formation of strings of particles at higher pre-shear strengths likely tend to delay the onset of extensional thickening, because the strings must be rotated from the shear direction in to extensional direction before strain-hardening can begin. A steep rise in steady-state Trouton ratio is observed for both 25 wt% and 30 wt% colloidal suspensions as a function of extension rate. For the 30 wt% case, the value of steady-state Trouton ratio is observed to increase an order of magnitude with a small change in extension rate. We believe that this observed rise in steady-state Trouton ratio is due to the additional rotational component present in shear flows.

A hyperbolic contraction was used to investigate the alignment and ordering of nano-particle suspensions in extensional flows through small-angle light scattering measurements. The alignment of clusters in the flow direction was demonstrated by the peak in the pixel intensity at 0 and 180 degrees. The strength of the peak and therefore the particle alignment was observed to increase with extension rate. In order to quantify the degree of alignment of the strings of particles, an alignment factor was calculated from the SALS patterns as a function of extension rate. The value of alignment factor is found to increase from 0 to 0.14. These results reinforce our physical interpretation of the extensional rheology measurements of 25 wt% colloidal suspensions of silica in polypropylene glycol.

Acknowledgements

The authors would like to thank the National Science Foundation for the generous support of this research under grant CBET-0547150 and the MRSEC and the CHM at the University of Massachusetts, Amherst.

References

1 J. Bender and N. J. Wagner, *J. Rheol.*, 1996, **40**, 899.
2 R. L. Hoffman, *J. Colloid Interface Sci.*, 1974, **46**, 491.
3 H. A. Barnes, *J. Rheol.*, 1989, **33**, 329.
4 J. F. Brady and G. Bossis, *J. Fluid. Mech.*, 1985, **155**, 105.
5 R. L. Hoffman, *J. Rheol.*, 1998, **42**, 111.
6 S. R. Raghavan and S. A. Khan, *J. Colloid Interface Sci.*, 1997, **185**, 57.
7 D. R. Foss and J. F. Brady, *J. Fluid. Mech.*, 2000, **407**, 167.
8 W. H. Boersma, J. Laven and H. N. Stein, *Aiche Journal*, 1990, **36**, 321.
9 B. J. Maranzano and N. J. Wagner, *J. Chem. Phys.*, 2001, **114**, 10514.
10 Y. S. Lee and N. J. Wagner, *Rheol. Acta*, 2003, **42**, 199.
11 C. Fischer, C. J. G. Plummer, V. Michaud, P. E. Bourban and J. A. E. Manson, *Rheol. Acta*, 2007, **46**, 1099.
12 R. Helber, F. Doncker and R. Bung, *J. Sound Vibration*, 1990, **138**, 47.
13 H. M. Laun, R. Bung and F. Schmidt, *J. Rheol.*, 1991, **35**, 999.
14 G. Bossis and J. F. Brady, *J. Chem. Phys.*, 1984, **80**, 5141.
15 G. Bossis and J. F. Brady, *J. Chem. Phys.*, 1989, **91**, 1866.
16 M. E. Fagan and C. F. Zukoski, *J. Rheol.*, 1997, **41**, 373.
17 B. J. Maranzano and N. J. Wagner, *J. Rheol.*, 2001, **45**, 1205.
18 H. M. Laun, R. Bung, S. Hess, W. Loose, O. Hess, K. Hahn, E. Hadicke, R. Hingmann, F. Schmidt and P. Lindner, *J. Rheol.*, 1992, **36**, 743.
19 A. A. Catherall, J. R. Melrose and R. C. Ball, *J. Rheol.*, 2000, **44**, 1.
20 W. H. Boersma, J. Laven and H. N. Stein, *J. Colloid Interface Sci.*, 1992, **149**, 10.
21 J. Mewis and G. Biebaut, *J. Rheol.*, 2001, **45**, 799.
22 Y. S. Lee, E. D. Wetzel and N. J. Wagner, *J. Mater. Sci.*, 2003, **38**, 2825.
23 J. W. Bender and N. J. Wagner, *J. Colloid Interface Sci.*, 1995, **172**, 171.
24 J. H. Xu, S. Chatterjee, K. W. Koelling, Y. R. Wang and S. E. Bechtel, *Rheol. Acta*, 2005, **44**, 537.
25 A. W. K. Ma, F. Chinesta, T. Tuladhar and M. R. Mackley, *Rheol. Acta*, 2008, **47**, 447.
26 G. K. Batchelor, *J. Fluid Mech.*, 1971, **46**, 813.
27 E. S. G. Shaqfeh and G. H. Fredrickson, *Phys. Fluids A: Fluid Dynamics*, 1990, **2**, 7.
28 J. P. Rothstein and G. H. McKinley, *J. Rheol.*, 2002, **46**, 1419.
29 J. P. Rothstein, *J. Rheol.*, 2003, **47**, 1227.
30 S. L. Anna and G. H. McKinley, *J. Rheol.*, 2001, **45**, 115.
31 G. H. McKinley and T. Sridhar, *Ann. Rev. Fluid Mech.*, 2002, **34**, 375.
32 V. Tirtaatmadja and T. Sridhar, *J. Rheol.*, 1993, **37**, 1081.
33 S. L. Anna, G. H. McKinley, D. A. Nguyen, T. Sridhar, S. J. Muller, J. Huang and D. F. James, *J. Rheol.*, 2001, **45**, 83.
34 M. S. N. Oliveira, M. A. Alves, F. T. Pinho and G. H. McKinley, *Experiments in Fluids*, 2007, **43**, 437.
35 J. P. Rothstein, *J. Rheol.*, 2003, **47**, 1227.
36 D. M. Jones, K. Walters and P. R. Williams, *Rheol. Acta*, 1987, **26**, 20.
37 A. Bhardwaj, D. Richter, M. Chellamuthu and J. P. Rothstein, *Rheol. Acta*, 2007, **46**, 861.
38 R. G. Larson, *J. Non-Newtonian Fluid Mech.*, 2000, **94**, 37.
39 S. L. Anna and G. H. McKinley, *Rheol. Acta*, 2008, **47**, 841.
40 R. Scirocco, J. Vermant and J. Mewis, *J. Non-Newtonian Fluid Mech.*, 2004, **117**, 183.
41 B. J. Maranzano and N. J. Wagner, *J. Chem. Phys.*, 2002, **117**, 10291.
42 L. M. Walker, W. A. Kernick and N. J. Wagner, *Macromolecules*, 1997, **30**, 508.

